J. Membrane Biol. 84, 81–95 (1985)

The Journal of
Membrane Biology

Spin Probe Clustering in Human Erythrocyte Ghosts

Larry M. Gordon*, Frank D. Looney† and Cyril C. Curtain†
* Rees-Stealy Research Foundation, San Diego, Calif. 92101
and † Biotechnology Section, Division of Chemical and Wood Technology, CSIRO, Clayton, Victoria 3168, Australia

Summary. A model has been developed for 5-nitroxide stearate, I(12,3), distribution in human erythrocyte ghosts which accurately predicts ESR spectral alterations observed with increased probe/total lipid (P/L) at 37°C. This spin probe occupies a class of high-affinity, noninteracting sites at low loading. Saturation occurs with increasing probe concentration, and, at higher loading, the probe inserts itself at initially dilute sites to form membrane-bound clusters of variable size. No 'low' probe remains at high P/L where all I(12,3) clusters in a 'concentrated' phase. This model allows determination of the dilute/clustered probe ratio, and shows that I(12,3) segregates in erythrocytes at what might otherwise be considered low P/L (e.g., 1/359). These findings validate the earlier use of empirical parameters to estimate probe sequestration in biological membranes.

Key Words erythrocyte ghosts · spin probe · radical interactions · lipid domains · fluidity · electron spin resonance

Introduction

Alterations in ESR[1] spectra due to probe-probe interactions have been reported in a wide range of spin-labeled biological membranes (for review *see* Ref. [7]). At sufficiently high loading, probe concentration-dependent effects characteristically perturb the order parameters and polarity of the 5-nitroxide stearate spin probe, I(12,3), in rat heart plasma membranes [20, 33], rat liver plasma membranes [16, 18, 28, 33], human lymphocytes [8], rat mast cells [11], rat fat-cell ghosts and plasma membranes [1, 34], human platelet plasma membranes [18, 35], erythrocytes [4, 5, 16], microsomal membranes from *Acanthamoeba castellani* [30], mouse mastocytoma cells [29], rat macrophages [24], human lens [31], renal brush-border membranes of rabbit [13], and outer membranes of *Dunaliella salina* [9]. The nature of the spectral changes suggested that these effects were not due to perturbations in membrane structure, but were a consequence of radical interactions resulting from spin probe clustering [7, 20]. Several empirical parameters [e.g., the inner hyperfine splitting ($2T_\perp$) and the peak-to-peak width of the central line (Δ)H] were used to estimate nitroxide radical interactions in labeled membranes [20, 33].

Despite the utility of empirical parameters in following spin-probe clustering in biomembranes [7, 8, 10, 16, 18, 20], this approach suffers from inherent limitations. Such parameters do not indicate whether all or just a fraction of the probe segregates. No definitive information is provided on relationships between the respective environments of clustered and unclustered probe. Moreover, little is known concerning the ability of sequestered probe to perturb the surroundings of any unclustered probe. The absence of a detailed physical model for probe clustering has prevented us from quantitatively predicting the spectral broadening seen at high loading.

Here, the ESR spectra of I(12,3)-labeled human erythrocyte ghosts have been interpreted in terms of two components: i) noninteracting, or 'low' probe and ii) clustered, or 'concentrated' probe. Assuming that the exchange-rate between the probe in 'clustered' and 'low' states is slow on the ESR timescale (10^{-8} sec), spectral subtractions have been performed to artificially generate the alterations seen upon probe addition, and to quantitatively analyze relative proportions of concentrated and dilute probe. This empirical procedure is similar in principle to that used earlier to determine lipid-water partition coefficients for a probe [7].

[1] Abbreviations used: ESR, electron spin resonance; I(12,3), the N-oxyl-4′,4′-dimethyloxazolidine derivative of 5′-ketostearic acid; P/L, ratio of probe molecules to total lipid molecules; dil, 3,3-dioctadecylindocarbocyanine; NBD-PE, N-(7-nitro-2,1,3-benzoxadiazol-4-yl)phosphatidylethanolamine; NBD-Chol, N^1-cholesterylcarbamoyl-N^8-(7-nitro-2,1,3-benzoxadiazol-4-yl)-3,6-dioxaoctane-1,8-diamine; L_D, lateral diffusion coefficient (cm^2/sec).

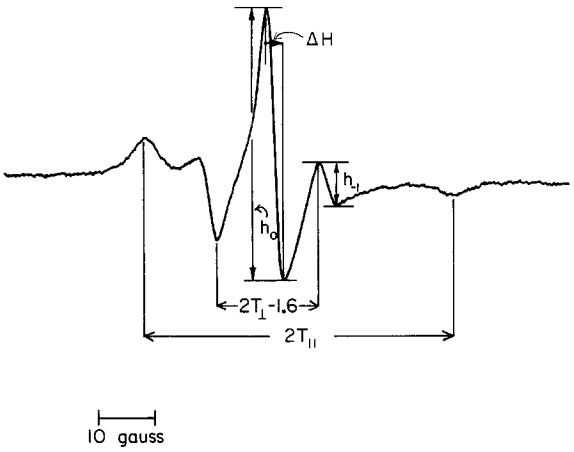

Fig. 1. ESR spectrum of I(12,3)-labeled human erythrocyte ghosts at 37°C, recorded using a Varian V-4502 spectrometer with a 5-min scan time, 800 receiver gain, 2G modulation amplitude, 10-mW microwave power, and 1-sec time-constant. Outer and inner hyperfine splittings, $2T_\parallel$ and $2T_\perp$ were measured as shown; $2T_\perp$ was corrected by addition of 1.6 G [19]. The peak-to-peak distance of the central line (ΔH) is indicated. Respective heights of the central line (h_0) and the high-field peak of the inner hyperfine doublet (h_{-1}) are shown. The μg probe/mg protein and P/L ratios, determined from the number of paramagnetic spins in the spectrum were 0.11 and 1/4600, respectively (*see* Materials and Methods and Ref. [36])

Materials and Methods

Materials

I(12,3) was obtained from Syva Co., Palo Alto, Calif., and thin-layer chromatographic analysis indicated negligible impurities. All other reagents were obtained from Sigma Chemical Co., St. Louis, Mo.

Preparation of Human Erythrocyte Ghosts

Ghosts were obtained from human erythrocytes according to Dodge et al. [12] and suspended in 100 mM Tris, pH 7.4, at 12, 42 or 83 mg protein/ml. Samples were used either fresh or after storage at −20°C. Protein was determined from micro-Kjeldahl or dry weight measured by heating 250-μl aliquots for 120 min at 105°C. Ghosts were assumed to be 50% protein and 50% lipid on a weight basis.

Membrane Spin-Labeling and Spectral Recording

I(12,3) was dissolved in ethanol (3×10^{-2} M) and aliquots were dried with a stream of dry N_2 gas in plastic vials or glass test tubes. Erythrocyte ghosts (60 to 80 μl) were added to the probe and gently vortexed for several min, at room temperature. Spin-labeled ghosts were syringed into 50 μl capillary pipettes (Drummond Scientific Co.) which were heat-sealed at one end. I(12,3) incorporation was tested by comparing the amount of probe added to ghost suspension (i.e., μg I(12,3)/mg protein 'wt') with the paramagnetic spins observed in the microwave cavity (i.e., μg I(12,3)/mg protein 'spins'). The number of spins was calculated from the ratio of the double integrated spectrum of I(12,3)-labeled erythrocyte ghosts with that of the Varian strong-pitch reference (0.1% pitch, with 3×10^{15} spins in 5.5. mm). The spin-label/membrane ratios for probe in the cavity were 0.03 to 45 μg I(12,3)/mg erythrocyte protein (or 1 probe per 16,000 to 9.3 lipid). The P/L was calculated assuming all lipid to the phospholipid and cholesterol [12].

ESR spectra were recorded with either a Varian V4502 spectrometer fitted with a Deltron (Sydney) Model DCM 20 temperature control accessory or a Varian E-104A spectrometer equipped with a temperature regulator. Pipettes containing the samples were placed in a special holder (attributed by Gaffney to R. Kornberg [14]) which was mounted in the temperature accessory. The V4502 spectrometer was interfaced to a Hewlett-Packard 9825A computer through a Hewlett-Packard 3437A System Voltmeter, while spectra recorded on the E-104A were digitized with a Hewlett-Packard 7470A plotter and 9816 computer. Additions, subtractions and integrations were performed on stored data. Figure 1 is a spectrum of I(12,3)-labeled erythrocyte ghosts.

Evaluation of the Flexibility of the Membrane-Incorporated I(12,3) Probe

The following order parameters may be used to assess the flexibility of the fatty-acid spin probe:

$$S(T_\parallel) = \frac{1}{2}\left[\frac{3(T_\parallel - T_{xx})}{(T_{zz} - T_{xx})} - 1\right] \quad (1)$$

$$S(T_\perp) = \frac{1}{2}\left[\frac{3[(T_{zz} + T_{xx}) - 2T_\perp]}{(T_{zz} - T_{xx})} - 1\right] \quad (2)$$

$$S = \frac{(T_\parallel - T_\perp)}{(T_{zz} - T_{xx})}\frac{(a_N)}{(a'_N)}. \quad (3)$$

$T_\parallel$ and $T_\perp$ for the membrane-incorporated probe are the hyperfine splitting elements parallel and perpendicular to z', the symmetry axis of the effective Hamiltonian (**H'**), while T_{xx} and T_{zz} are the splitting elements of the static interaction tensor (**T**) parallel to the static Hamiltonian (**H**) principal nuclear hyperfine axes x and z. Elements of **T** were determined by incorporating probe into host crystals: $(T_{xx}, T_{zz}) = (6.1, 32.4)$ G [7], and a_N and a'_N are the isotropic hyperfine coupling constants for the probe in membrane and crystal [i.e., $a'_N = \frac{1}{3}(T_\parallel + 2T_\perp)$ and $a_N = \frac{1}{3}(T_{zz} + 2T_{xx})$]. Increases in a'_N reflect a more polar environment.

If experimentally determined low probe concentrations are employed [33], $S(T_\parallel)$ and $S(T_\perp)$ are sensitive to membrane fluidity (or, more accurately, the flexibility of the incorporated probe). S, $S(T_\parallel)$ and $S(T_\perp)$ may assume values between 0 and 1, with the extremes indicating that the probe samples respectively fluid and immobilized environments. S, which requires both splittings, corrects for small polarity differences between the membrane and reference crystal. Although $S(T_\parallel)$ and $S(T_\perp)$ do not include polarity corrections, these expressions with certain limitations are useful fluidity approximations [7, 19].

Empirical Parameters Sensitive to Nitroxide Radical Interactions

Estimation of probe-probe interactions [7, 20, 33] was performed using four empirical parameters. The first involves measuring the peak-to-peak width of the central line (i.e., ΔH of Fig. 1),

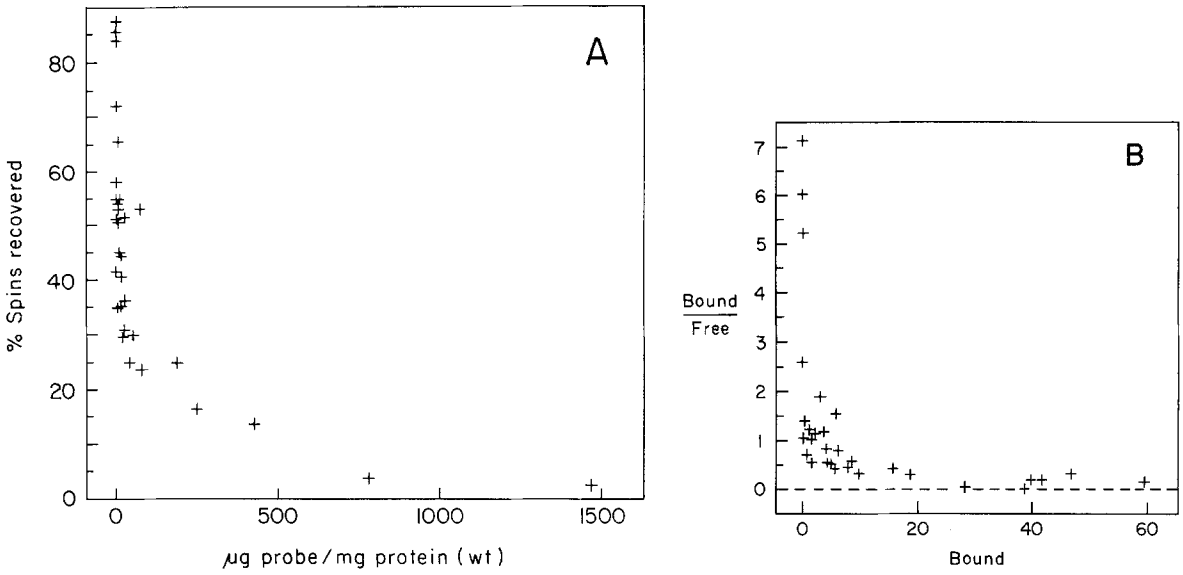

Fig. 2. I(12,3) uptake by erythrocyte ghosts. (*A*) Plot of % recovered spins *vs.* weight of probe added to 60 μl membrane aliquots. % Recovered spins was calculated from the ratio of the probe weight added to the sample (i.e., μg probe/mg protein 'wt') to that determined from the spins in the spectra (i.e., μg probe/mg protein 'spins'). (*B*) Scatchard plot, where BOUND = (nm probe/mg protein 'spins') and FREE = (nm probe/mg protein 'wt' − nm probe/mg protein 'spins'). (*See* Materials and Methods)

$$\Delta H = \Delta H_0 + \Delta H_{dip} + \Delta H_{ex} \quad (4)$$

where ΔH_0 is the linewidth without interactions, ΔH_{dip} is the line broadening caused by magnetic dipolar interactions and ΔH_{ex} is contributed by spin-spin exchange [7]. Enhanced probe-probe interactions increase ΔH [32, 36].

Second and third measures are based on the observation that $T_\perp$, but not $T_\parallel$, broadens with increasing P/L in various membranes, including erythrocyte ghosts [7, 8, 16, 33]. For those probe concentrations where the percentage change in $S(T_\parallel)$, $\Delta S(T_\parallel)$ is zero, decreases in $S(T_\perp)$ reflect enhanced radical interactions. Another way to express this relationship is through the m parameter [7, 10, 33]

$$m = \frac{(T_\parallel - a'_N)}{(T_\parallel - a_N)}. \quad (5)$$

If the polarity of the membrane (a'_N) is identical to that of the host crystal (a_N) and probe interactions are absent, then $m = 1$. If probe-probe interactions increase $2T_\perp$, then m will be increasingly less than 1.

The fourth parameter depends on the height of the high-field peak of the inner hyperfine doublet (h_{-1} in Fig. 1) decreasing with respect to that of the central line (h_0): h_{-1}/h_0 declines as the probe concentration is elevated [7, 20].

Results and Discussion

Spin-Labeling of Erythrocyte Ghosts

I(12,3) incorporation was examined by comparing the weight of the probe added to the membrane sample with that calculated for the spins present in the spectrum (*see* Materials and Methods). Figure 2*A* shows that at low loading there is quantitative uptake of the probe by erythrocyte membranes. Above approx. 0.2 μg I(12,3)/mg protein 'wt', however, dramatically less probe is introduced into the cavity. One explanation of Fig. 2*A* lies in a limited capacity of the membrane to solubilize I(12,3) at high loading. This was confirmed by aspirating a ghost sample (60 μl) labeled with 437 μg I(12,3)/mg protein 'wt', and then washing the presumably empty vial three times with unlabeled ghost samples (100 μl of 83 mg/ml per wash). The μg probe/mg protein 'spins' for labeled and successively unlabeled samples were 14, 6, 7, 15, indicating that quantitative incorporation does not occur at such high loading. Instead, excess I(12,3) remains as a waxy deposit on the side of the tube.

One interpretation of Fig. 2*A* is that I(12,3) binds to human erythrocyte ghosts at specific membrane sites. Scatchard analysis indicates that I(12,3) interaction with ghosts cannot be viewed as a simple partitioning phenomenon of an infinitely dilute solute in an ideal solvent (Fig. 2*B*). For low levels of bound probe, I(12,3) apparently binds to a single class of sites with high affinity. If only bound μg probe/mg protein ratios less than 2 are considered, these sites yield an apparent association constant (K_a) of 6.3×10^8 mg protein/M and the number of sites/mg protein is 3.2×10^{15}. However, the I(12,3)-binding isotherm exhibits such significant curvature at high loading (Fig. 2*B*) that probe uptake is re-

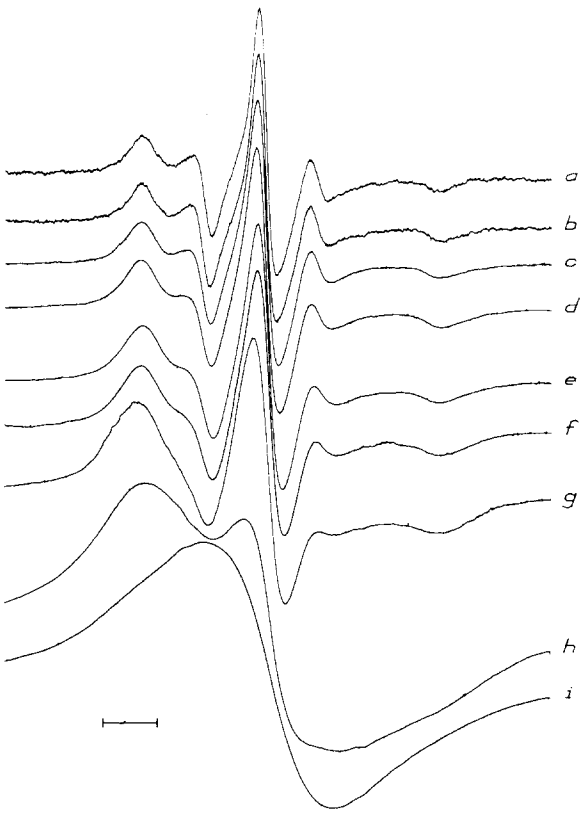

Fig. 3. ESR spectra of human erythrocyte ghosts at 37°C labeled with varying concentrations of I(12,3). Probe/lipid (μg probe/mg protein) ratios were: (*a*) 1/4600 (0.11); (*b*) 1/2250 (0.22); (*c*) 1/359 (1.37); (*d*) 1/188 (3.28); (*e*) 1/119 (4.05): (*f*) 1/90 (6.08); (*g*) 1/38 (12.9); (*h*) 1/20 (30); and (*i*) 1/9.3 (45). Three major P/L ranges may be defined: 'low', from 1/4600 to less than 1/2250; 'intermediate', from 1/2250 to 1/38; and 'very high', above 1/38 (*see* text). Figure 3*i* is defined as 'pure' phase. The horizontal bar indicates 10 gauss

duced. One explanation for this behavior is that I(12,3) binds to two classes of independent sites (i.e., "low" and "high" affinity sites). Alternatively, probe-membrane sites when occupied at high loading may act, perhaps through a cooperative mechanism, to inhibit further I(12,3) binding. It is, unfortunately, not possible to distinguish between these models by simply examining Fig. 2.

All of the probe/lipid (or μg probe/mg protein) ratios used in the following experiments were determined by calculating paramagnetic spins from the spectrum.

Effects of I(12,3) Concentration on Spectra of Human Erythrocyte Ghosts

The ESR spectrum of erythrocyte ghosts labeled with I(12,3) at a low P/L of 1/4600 (Fig. 3*a*) shows that the probe undergoes rapid anisotropic motion about its long molecular axis at physiologic temperatures. The spectrum at 1/4600 was identical to that at 1/16,000, indicating that 1/4600 is in the 'low' range. In the 'intermediate' range of 1/2250 to 1/38, raising the P/L decreased h_{-1} with respect to h_0, displaced downward the high-field baseline and upward the low-field baseline, increased $2T_\perp$ and ΔH, and left $2T_\parallel$ unchanged (Fig. 3*b—g*). Increasing the P/L above 1/38 achieves a 'very high' range, identified by noticeably broadened spectra and sloping baseline (Fig. 3*h,i*). Measurements of hyperfine splittings and ΔH were either difficult or impossible in this range. At these high membrane concentrations, no 'liquid-lines' due to I(12,3) tumbling rapidly in aqueous solution were present. Similar spectral alterations have been reported with I(12,3)-labeled whole erythrocytes [5] or erythrocyte ghosts [16, 39].

I(12,3) Concentration Effects on Erythrocyte Ghost Order Parameters and Empirical Parameters Sensitive to Radical Interactions

For 'low' P/L less than 1/2250, increasing the I(12,3) concentration did not affect S, $S(T_\parallel)$ or $S(T_\perp)$. As the probe concentration was elevated in the 'intermediate' range, however, S and $S(T_\perp)$ decreased substantially while $S(T_\parallel)$ was constant (Fig. 4*A*). These order parameter effects are most likely due to enhanced radical interactions and not membrane fluidization. The broadening of $T_\perp$ [and decrease in $S(T_\perp)$] was closely correlated with decreases in m and increases in ΔH (Fig. 4); earlier investigations have demonstrated that radical interactions broaden the ΔH of labeled model and biological membrane [7, 33]. Reductions in S and $S(T_\perp)$ were also associated with such characteristic exchange-broadening effects as the decrease in the high-field peak of the inner hyperfine doublet (h_{-1}) and the downward displacement of the high-field baseline (Fig. 3*b-g*). The finding that $T_\parallel$ [and $S(T_\parallel)$] is unaltered for erythrocyte membranes in the intermediate range (Fig. 4*A*) indicates that the "apparent" increase in fluidity with probe concentration, denoted by reductions in S and $S(T_\perp)$, is not the result of probe-mediated perturbations; any fluidization allowing more probe flexibility requires that $T_\parallel$ narrow commensurately with increases in $2T_\perp$ and h_{-1}/h_0 and that ΔH decreases.

Analogous $I(m,n)$ concentration effects on order parameters and ΔH have been observed in many other biological membranes (for review, *see* Ref. [7] and Introduction). In previous experiments on I(12,3)-labeled erythrocyte ghosts (Fig. 2 of Ref. [16]), these parameters depended similarly on probe

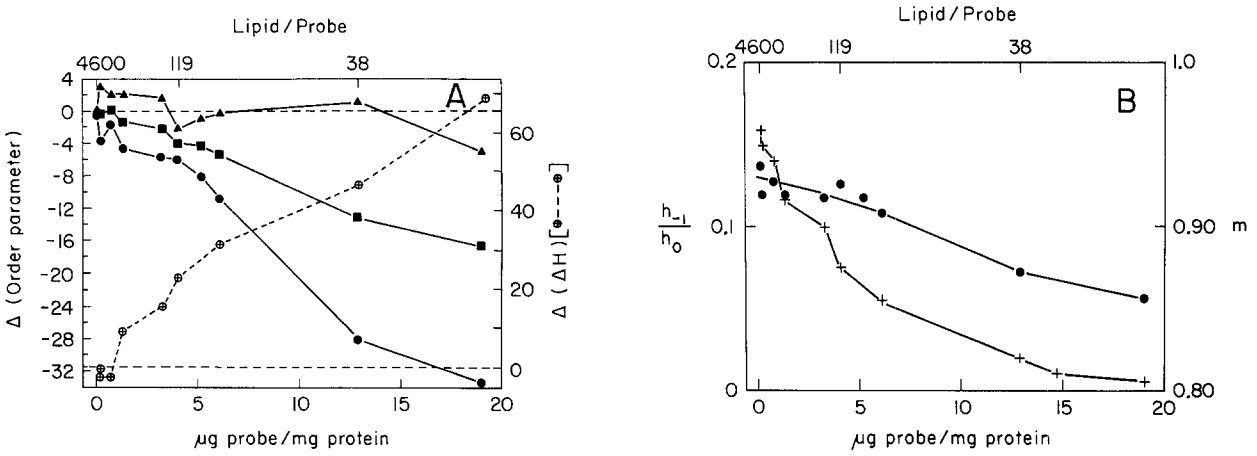

Fig. 4. Effects of I(12,3) concentration on order parameters and empirical parameters sensitive to probe-probe interactions at 37°C. (*A*) $\Delta S(T_{\parallel})$ [▲], $\Delta S(T_{\perp})$ [●] and ΔS [■] are percent changes from baseline values measured at P/L = 1/4600. Control $S(T_{\parallel})$, $S(T_{\perp})$, and S were 0.720, 0.583 and 0.640. Δ (ΔH) [⊕] is percent change in ΔH from the baseline value of 3.73 G. (*B*) h_{-1}/h_0 [+] as shown in Fig. 1 and m [●] from Eq. [5]

concentration. One important difference, however, lies in our present finding that radical interactions occur at much lower P/L. We attribute this discrepancy to the incorrect implicit assumption of Gordon and Mobley [16] that I(12,3) quantitatively incorporates into erythrocyte ghosts at all P/L. Indeed, both order parameter and ΔH *vs.* probe concentration plots are in good agreement, once Fig. 2 has been used as a calibration curve to correct Fig. 2 of Gordon and Mobley [16] for the number of spins present in the cavity.

It is unlikely that the probe effects in Figs. 3 and 4 are due to increased ΔH_{dip}, but are instead the result of enhanced ΔH_{ex} arising from I(12,3) clustering. This is because the probe executes rapid anisotropic motion at 37°C and dipole-dipole interactions are relatively long-range, tending to be averaged out by rapid diffusion and/or tumbling, while exchange interactions require that labels be in van der Waal's contact and decrease rapidly with distance.

Figure 4 indicates that $S(T_{\perp})$, m, ΔH and h_{-1}/h_0 are responsive to enhanced interactions, with ΔH and h_{-1}/h_0 being more sensitive. However, monitoring this phenomenon with empirical parameters is subject to several limitations. First, the parameters cannot be accurately determined for P/L >1/38 (Fig. 3*h,i*). Despite this difficulty, there is little doubt that radical interactions are more extensive in the 'very-high' range as these spectra predominantly feature single broad lines characteristic of extensive radical interactions. A more important problem associated with relying solely on empirical parameters is that they do not provide additional details on the probe sequestration occurring in the membrane.

Physical Models of Membrane-Probe Distribution to Account for Spectra of I(12,3)-Labeled Human Erythrocyte Ghosts

Since I(12,3) uptake in the intermediate range is not due to probe binding to a single class of independent sites, Fig. 3*b—g* may be composite spectra arising from probe molecules in discrete environments. If exchange between these states is slow on an ESR time scale (approx. 10^{-8} sec), several physical models of membrane-probe distribution may be tested by adding or subtracting experimental spectra. The validity of these (or any) models rests on their ability to simulate experimental spectra.

Probe Distribution Model I: Magnetically Dilute Probe Yielding 'Low' Spectra in Equilibrium with Highly Clustered Probe Yielding Single Broad-Line Spectra

Erythrocyte ghosts have only limited sites in the bilayer that can be occupied by I(12,3), 'Low-range' spectra (Fig. 3*a*) reflect the environment of I(12,3) in these sites. As the I(12,3) concentration increases and the sites fill, a phase of pure (or, at least, very concentrated) probe arises. Intermediate range spectra (Fig. 3*b—g*) would consist of two components: (i) an anisotropic spectrum reflecting magnetically dilute probe molecules in membrane sites (e.g., Fig. 3*a*); and (ii) a single broad line ('pure' phase spectrum) representing I(12,3) in concentrated micelles or patches (e.g., Fig. 3*i*). Model I assumes that only I(12,3) in state (ii) contributes to radical interaction effects in the intermediate range

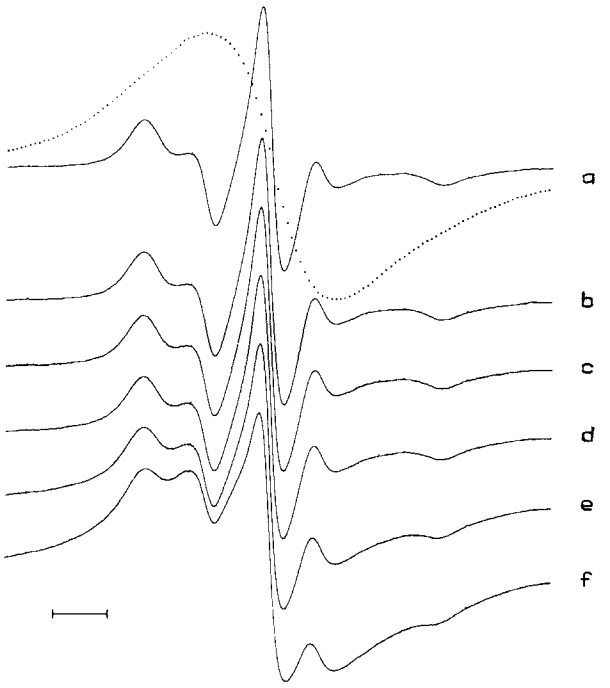

Fig. 5. Addition ESR spectra of human erythrocyte ghosts to test Model I, obtained by mixing a single broad line (or 'pure' phase spectrum) with an intermediate-range spectrum. (*a*) Experimental spectra obtained from ghosts labeled with either an intermediate P/L = 1/188 (solid line) or a very-high (i.e., 'pure') P/L = 1/9.3 (dashed line). (*b*) 20% Pure, calculated from % Pure = 200 · [Npure/(Npure + Ninter)], where Npure = spins in pure spectrum and Ninter = number of spins in intermediate spectrum. % Intermediate = 100 − % Pure. (*c*) 40% Pure; (*d*) 60% Pure; (*e*) 80% Pure; and (*f*) 90% Pure. The horizontal bar indicates 10 gauss

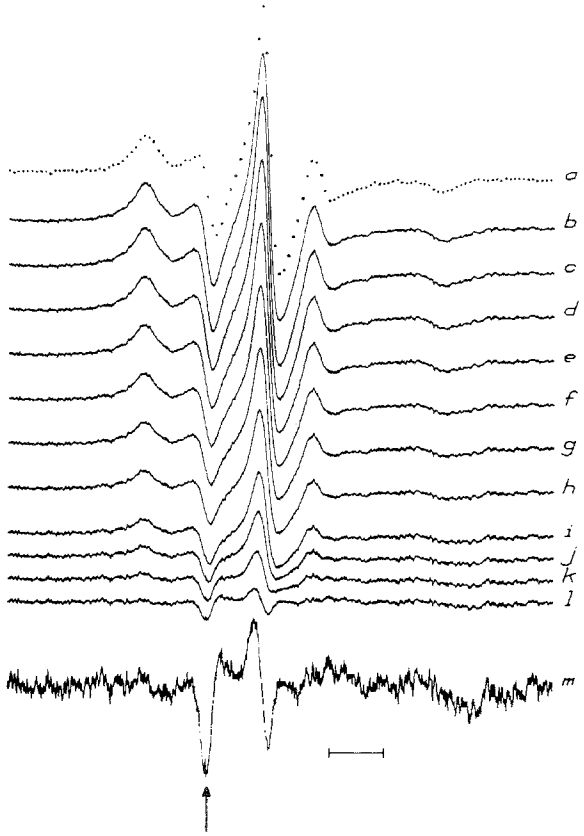

Fig. 6. Subtraction spectra to test Model II, obtained by subtracting incremental amounts of an experimental low-range spectrum [P/L = 1/4600; dotted line in (*a*)] from an experimental intermediate-range spectrum [P/L = 1/2250; solid line in (*b*)]; h_0 of (*a*) is normalized to that of (*b*). (*c*), (*d*), (*e*), (*f*), (*g*) and (*h*) are intermediate spectra remaining after subtracting low increments of: 0.1, 0.2, 0.3, 0.4, 0.5 and 0.6. (*i*) Remaining spectrum after subtracting 0.7 · LOW. This is the endpoint of the spectral subtraction as defined in the text. ('Dilute') and ('Concentrated') probe are 91 and 9%, calculated as in Results and Discussion. (*j*), (*k*) and (*l*) are intermediate spectra remaining after subtracting low increments of 0.8, 0.9 and 1.0. These are oversubtracted, as indicated by the descent of the low-field peak of the inner hyperfine doublet (*see* arrow). (*m*) is four times that of (*i*) and the arrow indicates the appearance of the 'low' spectrum in inverted phase due to oversubtraction. The horizontal bar indicates 10 gauss

(Fig. 3*b*—*g*). It also assumes that clustered probe does not perturb 'magnetically dilute' I(12,3). Model I is similar to the 'patch' model suggested earlier to explain the spectra observed with I(12,3)-labeled rat heart plasma membranes [20].

Model I was tested by mixing varying proportions of 'pure' phase spectrum (Fig. 3*i*) with either 'low' or 'intermediate' range spectra. Simulated spectra in Fig. 5 were obtained by adding the 'pure' phase spectrum to that of erythrocyte ghosts labeled with P/L = 1/188. As 'pure' phase increases, addition spectra share only some of the alterations seen in the intermediate range (Fig. 3*b-g*). Both the experimental and simulated spectra show depressed high-field baselines, elevated low-field baselines, increased ΔH, and slightly lowered $2T_{\parallel}$ at either high loading (Fig. 3*f,g*) or high percent 'pure' (Fig. 5*d*—*f*). Nevertheless, addition spectra are unable to mimic other experimental spectral perturbations. For example, $2T_{\perp}$ decreases with increasing 'pure' instead of increasing, and h_{-1}/h_0 is unaffected when it should be decreasing (Fig. 4*B*), even when 'pure' is in excess of 80% (Fig. 5*e,f*). Although the separation of I(12,3) into clusters yielding single broad lines cannot be responsible for intermediate-range spectral alterations, we cannot exclude its occurrence in the 'very-high' range of Fig. 3.

Probe Distribution Model II: Magnetically Dilute Probe Yielding Low-Range Spectra in Equilibria with Clustered Probe Yielding Broadened Spectra

According to this model, intermediate spectra (Fig. 3*b*—*g*) consist of two components: (i) an anisotropic

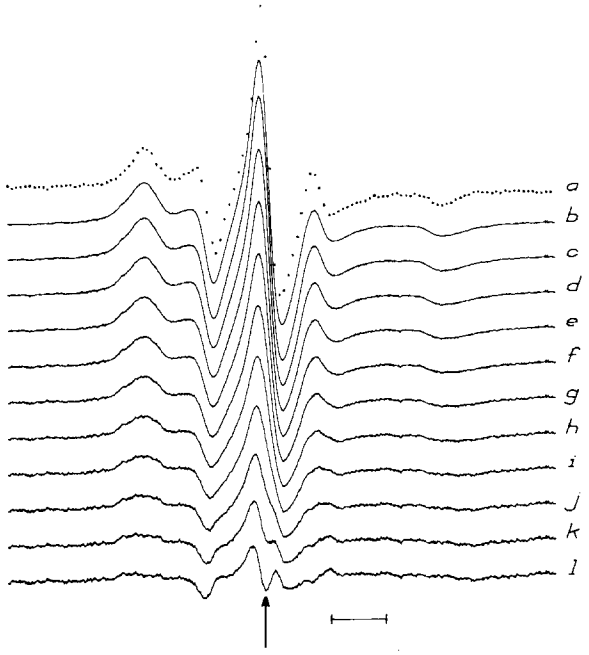

Fig. 7. Subtraction spectra to test Model II, obtained by subtracting incremental amounts of an experimental low-range spectrum [P/L = 1/4600; dotted line in (*a*)] from an experimental intermediate-range spectrum [P/L = 1/359; solid line in (*b*)]; h_0 of (*a*) is normalized to that of (*b*). (*c*), (*d*), (*e*), (*f*), (*g*) and (*h*) are intermediate spectra remaining after subtracting low increments of: 0.1, 0.2, 0.3, 0.4, 0.5 and 0.6. (*i*) Remaining spectrum after subtracting 0.7 · LOW. This is the endpoint of the subtraction as defined in the text. ('Dilute') and ('Concentrated') probe are 56 and 44%. (*j*), (*k*) and (*l*) are intermediate spectra remaining after subtracting low increments of 0.8, 0.9 and 1.0. These are oversubtracted, as indicated by the asymmetry of the central band and appearance of a shoulder due to 'low' spectrum in inverse phase [*see* arrow in (*l*)]. The horizontal bar indicates 10 gauss

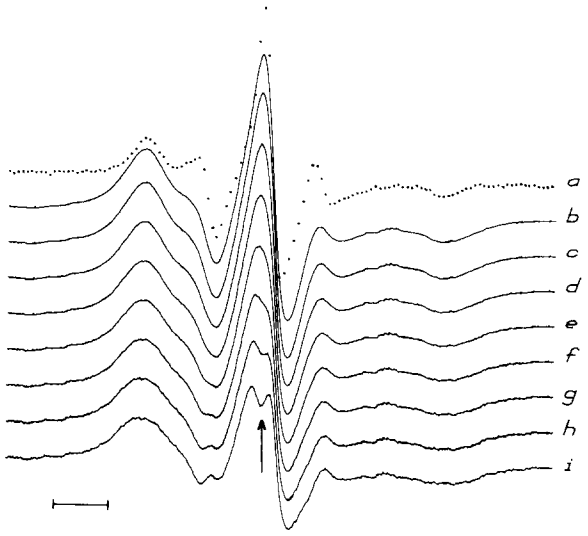

Fig. 8. Subtraction spectra to test Model II, obtained by subtracting incremental amounts of an experimental low-range spectrum [P/L = 1/4600; dotted line in (*a*)] from an experimental intermediate-range spectrum [P/L = 1/90; solid line in (*b*)]; h_0 of (*a*) is normalized to that of (*b*). (*c*) and (*d*) are intermediate spectra remaining after subtracting low increments of: 0.1 and 0.2. (*e*) Remaining spectrum after subtracting 0.3 · LOW. This is the endpoint of the subtraction as defined in the text. ('Dilute') and ('Concentrated') probe are 9 and 91%. (*f*), (*g*), (*h*) and (*i*) are intermediate spectra remaining after subtracting low increments of 0.4, 0.5, 0.6 and 0.7. These are oversubtracted, as indicated by the appearance of central band asymmetry and shoulder due to 'low' spectrum in inverse phase [*see* arrow in (*i*)]. The horizontal bar indicates 10 gauss

spectrum reflecting magnetically dilute probe molecules occupying membrane sites (Fig. 3*a*); and (ii) 'concentrated' spectra that do not necessarily reflect a unique species (e.g., 'pure' phase) but instead represent variable-sized probe clusters. Model II presumes that probe-exchange between 'dilute' and 'concentrated' sites is slow on an ESR time-scale, but makes no implicit assumption about the nature of 'concentrated' spectra.

The model was tested by subtracting incremental amounts of a low-range spectrum (P/L = 1/4600) from an intermediate spectrum (1/2250). Figure 6*c*—*i* shows that the 'subtracted' spectra accurately mimic those alterations observed when I(12,3) is added experimentally to ghosts initially labeled with a P/L of 1/2250 (Fig. 3*b*-*g*). Namely, removing 'low' increased $2T_\perp$ and ΔH, decreased h_{-1}/h_0, but left $2T_\parallel$ unaffected. The titration endpoint was identified by noting that the low-field peak of the inner hyperfine doublet (*see* arrow in Fig. 6*m*) falls below the high-field peak of the central band. This is due to oversubtraction such that the low-range spectrum appears in inverse phase. The 'concentrated' spectrum is isolated as that which arises immediately before the descent of this low-field peak (Fig. 6*i*). Relative proportions of 'dilute' and 'concentrated' probe are assessed by double integration of component spectra (Fig. 6*i*). Due to similar component line-shapes (Fig. 6*a*,*i*), the range between obvious undersubtraction and oversubtraction is approx. 10 to 15% of the 'concentrated' component [22].

Application of this subtraction protocol to intermediate-range spectra at higher loading (P/L = 1/359, 1/90 or 1/38) also generated spectral changes (Figs. 7—9) which are seen experimentally with increases in the probe/lipid (Fig. 3*b*—*g*). Here, however, endpoints were indicated by the central band first becoming asymmetric and then a shoulder arising on its high-field side (Figs. 7—9). These effects were each due to over-subtraction such that the low-range spectrum appears in inverse phase. 'Concentrated' spectra were assigned as those immediately before central-band peak asymmetry and shoulder (Figs. 7*i*, 8*e*, 9*d*). The dissimilarities between the 'low' and 'concentrated' lineshapes were much greater at these high P/L, permitting

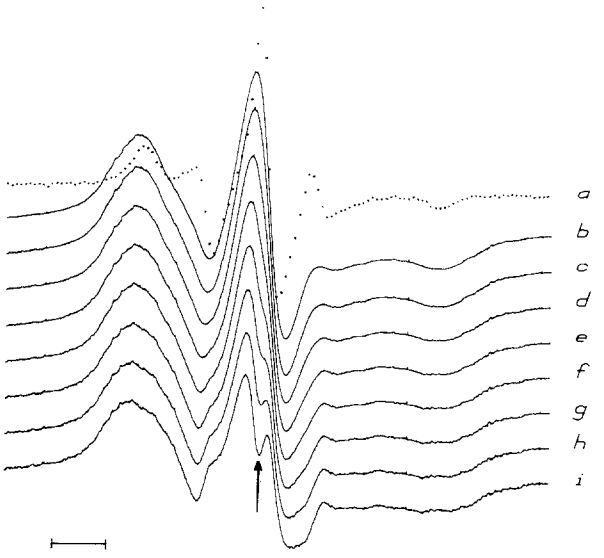

Fig. 9. Subtraction spectra to test Model II, obtained by subtracting incremental amounts of an experimental low-range spectrum [P/L = 1/4600; dotted line in (*a*)] from an experimental intermediate-range spectrum [P/L = 1/38; solid line in (*b*)]; h_0 of (*a*) is normalized to that of (*b*). (*c*) is an intermediate spectrum remaining after subtracting 0.1 · LOW. (*d*) Remaining spectrum after subtracting 0.2 · LOW. This is the endpoint of the subtraction, as defined in the text. ('Dilute') and ('Concentrated') probe are 4 and 96%. (*e*), (*f*), (*g*), (*h*) and (*i*) are intermediate spectra remaining after subtracting low increments of 0.3, 0.4, 0.5, 0.6 and 0.7. These are oversubtracted, as indicated by the asymmetry of the central band and appearance of a shoulder due to 'low' spectrum in inverse phase [*see* arrow in (*i*)]. The horizontal bar indicates 10 gauss

more precise estimates of 'dilute' the 'clustered' probe (i.e., approx. ± 1 to 2%). As P/L increased from 1/2250 to 1/38, the relative proportion of 'dilute' to 'concentrated' declined (Figs. 6—9, 14). Moreover, the absolute amount of 'dilute' probe decreased at high loading, since the fraction of low-range spectrum that could be removed without oversubtraction was reduced (Figs. 6—9, 15). It was not possible to remove any 'dilute' spectrum from a 'very-high' range spectrum (e.g., Fig. 3*h*) without oversubtracting, suggesting that only clustered probe exists at such high P/L.

Our initial working hypothesis for these data is that each probe occupies a single site under dilute conditions (Figs. 3*a*, 15*A*). High I(12,3) uptake at low loading in Fig. 2 is due to probe binding to a class of high-affinity sites. However, the elevated P/L in the intermediate range induce additional I(12,3) to insert itself at formerly dilute sites to produce clusters (Fig. 3*b—g*, 15*B—D*), causing an apparent loss of dilute sites. Curvature at high loading in the Scatchard plot of Fig. 2*B* is the result of probe binding to sites of lower affinity with variable association constants depending on the properties of the probe clusters. The enhanced probe-probe interactions detected by empirical parameters (Fig. 4*A,B*) would be a consequence of probe incorporating into already occupied membrane sites. At sufficiently high P/L (e.g., the very-high range of Fig. 3*h,i*), no 'dilute' probe is left and all the label is segregated (*see below*).

The ability of Model II to predict changes in S, $S(T_\parallel)$ and $S(T_\perp)$ is shown in Fig. 10. Until the respective titration endpoints are reached (*see* Figs. 6—9), subtracting increasing amounts of low-range spectrum from various intermediate-range spectra decreases $S(T_\perp)$ and, to a lesser extent, S, without significantly affecting $S(T_\parallel)$. These results are in good agreement with order parameter alterations observed experimentally in the intermediate range (Fig. 4*A*).

Model II is also able to simulate those perturbations in ΔH, h_{-1}/h_0 and m seen with increasing probe concentration in the intermediate range (Fig. 4*A,B*). Figure 11 was calculated from computer spectra generated by subtracting fractional amounts (X) of a low-range spectrum from spectra recorded at intermediate-range P/L. Experimental ΔH, m and h_{-1}/h_0 are shown at the −XLOW values of 0 in Fig. 11*A,B,C*, respectively. For each intermediate spectrum, subtracting the low-range spectrum changes the parameters in a manner similar to that found with increasing probe concentration (i.e., ΔH increased while m and h_{-1}/h_0 decreased).

'Concentrated' Spectra and Spectral Parameters, Obtained by Removing All 'Low' Component from Intermediate-Range Spectra According to Model II

The preceding results suggest that subtracting of low-range spectra from intermediate ones is a legitimate operation, since the spectral changes seen at higher probe loading are appropriately simulated. It then becomes important to carefully inspect intermediate-range spectra from which all low-range spectra have been subtracted, as these 'concentrated' spectra may provide information about the probe environment in the unsubtracted component. Figure 12 is a family of 'concentrated' spectra, obtained from experimental intermediate-range spectra following Model II. The 'concentrated' spectrum derived from P/L of 1/2250 (Fig. 12*a*) shows anisotropic properties, such as a well-defined inner splitting which indicates probe rotation about its long axis, and also broadened characteristics due to radical interactions. This suggests that 'concentrated' probe is membrane-bound and exists in a clustered state. Interestingly, increasing the P/L al-

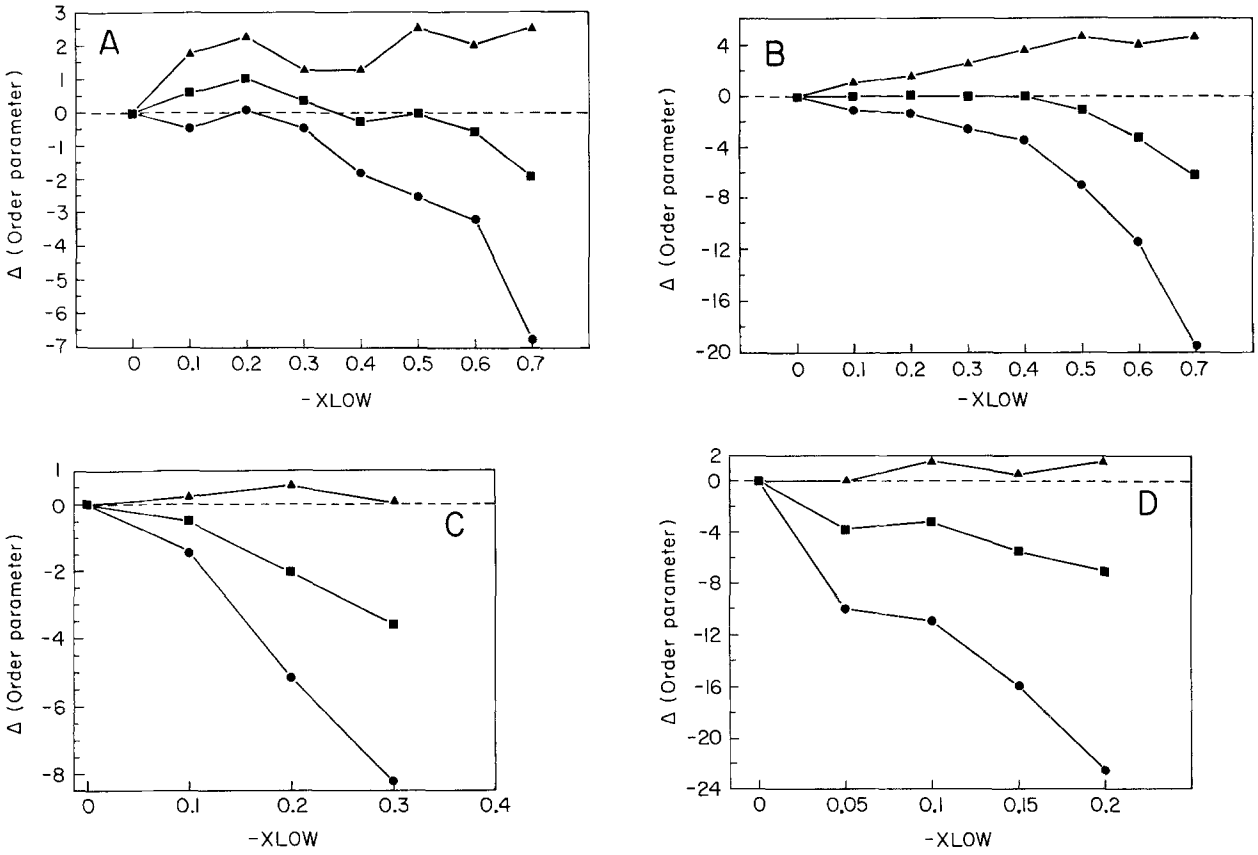

Fig. 10. Effects on order parameters $S(T_{\parallel})$ [▲], $S(T_{\perp})$ [●] and S [■] of subtracting a low-range spectrum (P/L = 1/4600) from intermediate-range spectra labeled with the following P/L: (*A*) 1/2250 (Fig. 6); (*B*) 1/359 (Fig. 7); (*C*) 1/90 (Fig. 8); and (*D*) 1/38 (Fig. 9). Δ (order parameter), the percent change in order parameter, is plotted as a fractional amount (X) of low-range spectrum (i.e., $X \cdot$ LOW), that was subtracted

ters the 'concentrated' spectra and associated parameters (i.e., $2T_{\perp}$ and ΔH increase, h_{-1}/h_0 decreases while $2T_{\parallel}$ remains unchanged) similarly to that observed with experimental intermediate-range spectra (Fig. 3*b*—*g*; Fig. 12). Moreover, plots of 'concentrated' Δ (order parameters) and Δ (ΔH) *vs.* probe concentration (Fig. 13) demonstrate alterations in agreement with those seen with intermediate-range spectra (Fig. 4*A*). These findings argue that the 'concentrated' component becomes more clustered as the P/L increases. The possibility that 'pure' phase is responsible for these changes was tested by adding 'pure' to a 'concentrated' spectrum. Since plots of Δ (order parameters) and Δ (ΔH) *vs.* % Pure (*not shown*) are unable to duplicate key parameter changes in Fig. 13, it seems improbable that 'pure' accounts for the spectral alterations observed in Fig. 12.

Our principal conclusion is that 'concentrated' spectra are due to clustered probe in the membrane. It is unlikely that 'concentrated' probe represents a unique component, given the spectral differences in Fig. 12. The absence of any common intersection points when Fig. 3 spectra are superimposed also argues against 'concentrated' spectra reflecting probe in a single environment. Such isoclinic points would normally result from isosbestic points in the absorption spectra, and would be indicative of equilibrium between probe in two well-defined states [22]. Instead, we propose that variations in Fig. 12 are due to differences in probe aggregation in the membrane. The finding that 'concentrated' spectra appear to be related would not be unexpected, as variable-sized clusters may be shared to some extent in the various 'concentrated' states. Hence, our definition of 'concentrated' spectra is operational, referring only to the contribution left after all 'dilute' is removed. The amount of clustering and probe-probe interactions in the 'concentrated' component ranges from minimal (Fig. 12*a*) to extensive (Fig. 12*g*). As is seen below, the ability of Model II to predict spectral changes seen at high loading in the intermediate range is somewhat limited by the 'concentrated' component not being unique.

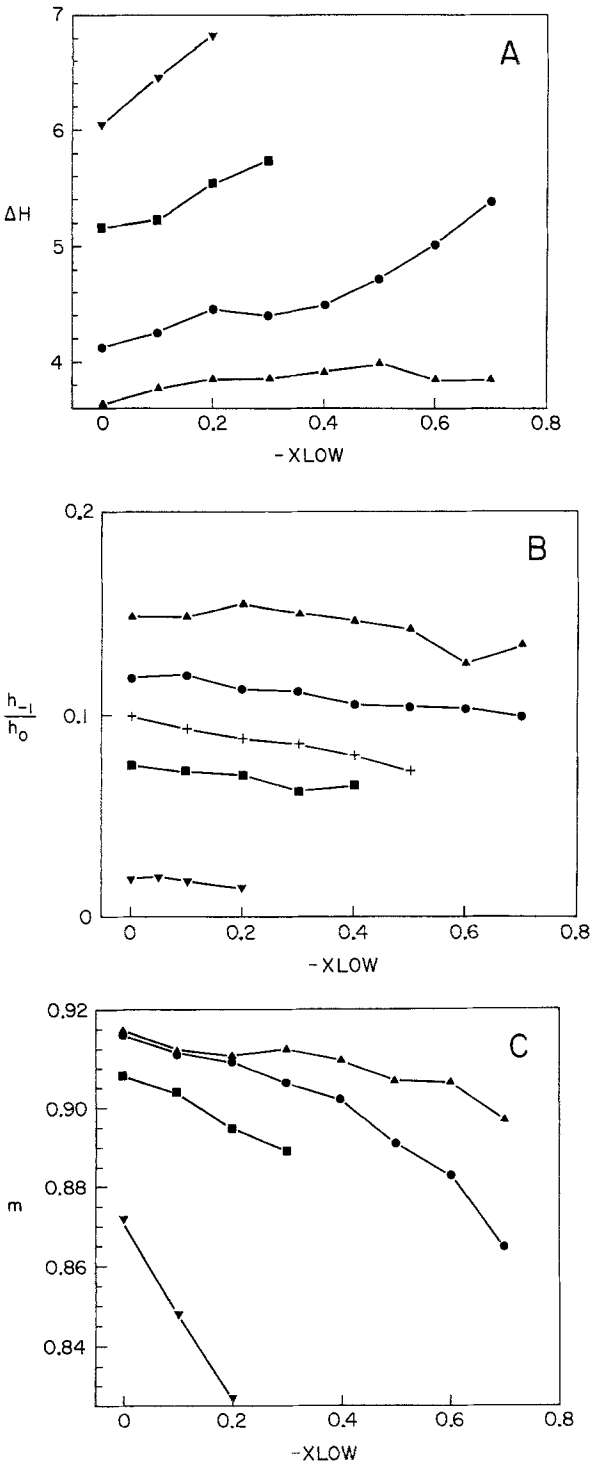

Fig. 11. Effects on ΔH, m and h_{-1}/h_0 of subtracting fractions (X) of a low spectrum (P/L = 1/4600) from intermediate spectra. (A) ΔH in gauss *vs.* $-X \cdot$ LOW, the fractional amount (X) of low-range that was subtracted; (B) h_{-1}/h_0 *vs.* $-X \cdot$ LOW; and (C) m *vs.* $-X \cdot$ LOW. Intermediate P/L were: 1/2250 [▲]; 1/359 [●]; 1/188 [+]; 1/90 [■]; and 1/38 [▼]. ΔH, h_{-1}/h_0 and m were calculated as described in the text

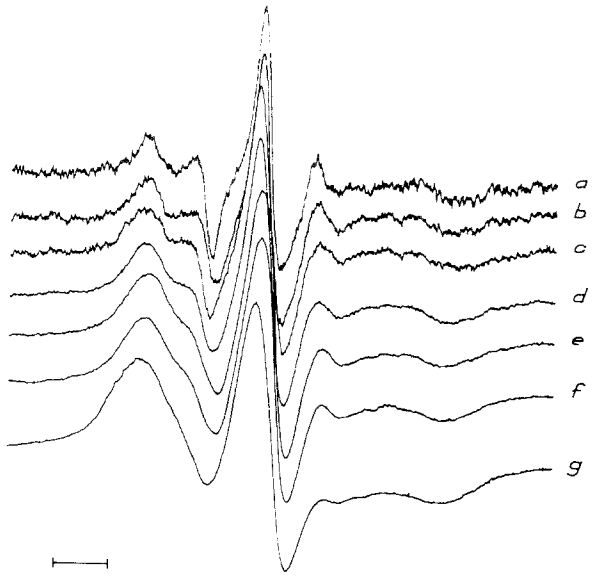

Fig. 12. 'Concentrated' spectra obtained by subtracting out all low component (P/L = 1/4600) from intermediate spectra recorded with the following P/L: (a) 1/2250; (b) 1/678; (c) 1/359; (d) 1/188; (e) 1/119; (f) 1/90; and (g) 1/38. The horizontal bar indicates 10 gauss

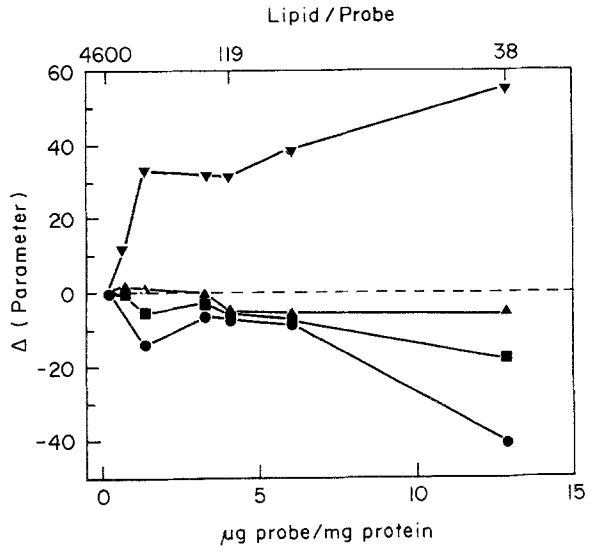

Fig. 13. Effects on 'concentrated' order parameters and ΔH of increasing the probe concentration. Probe concentration dependence of ΔS [■], $\Delta S(T_\perp)$ [●] and $\Delta S(T_\parallel)$ [▲], where Δ (order parameters) are percent changes from initial 'concentrated' values at P/L = 1/188. Baseline values for S, $S(T_\parallel)$, and $S(T_\perp)$ are 0.627, 0.732 and 0.551. Δ (ΔH) [▼] is the percent change in ΔH, determined from a control value of 4.39 G. 'Concentrated' spectra were determined as in Fig. 12

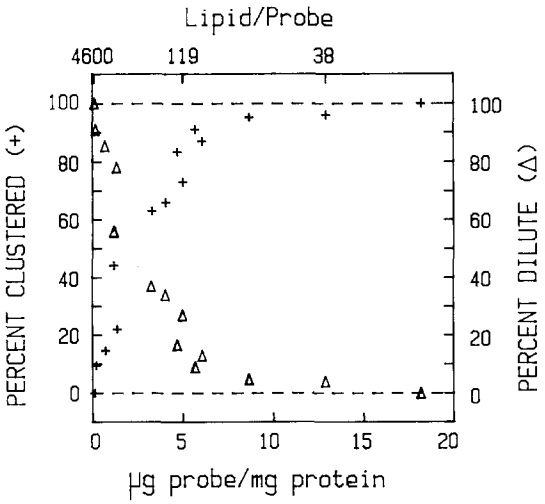

Fig. 14. Plot of the relative percentage of I(12,3) in 'clustered' and 'dilute' states as a function of probe concentration at 37°C. Clustered spins were calculated from that present in the concentrated spectrum, obtained at the titration endpoint of subtracting low-range spectrum (P/L = 1/4600) from intermediate-range spectra (e.g., Figs. 6*i*, 7*i*, 8*e*, 9*d*). 'Dilute' and 'concentrated' spins were assessed by double integration of component spectra. Subtraction of a spectrum obtained at a P/L of 1/16,000 from that of 1/4600 indicated only background noise, confirming that 1/4600 is 'magnetically dilute'

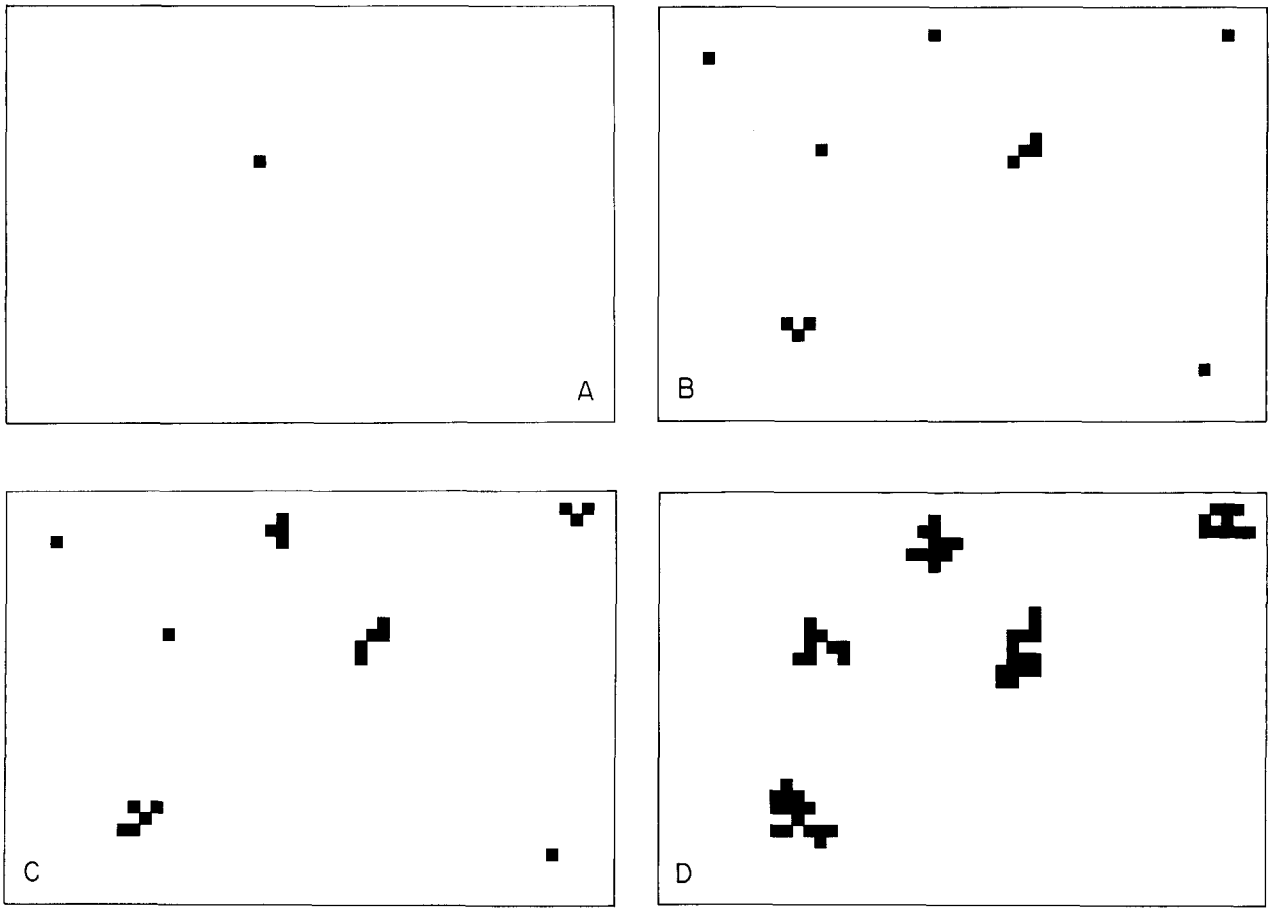

Fig. 15. Schematic of I(12,3) distribution in human erythrocyte ghosts, calculated from the data of Fig. 14 at the following P/L: (*A*) 1/4600 ('low'); (*B*) 1/359 ('intermediate'); (*C*) 1/90 ('intermediate'); and (*D*) 1/26 ('very high'). The diagram is a view perpendicular to the membrane bilayer. For illustrative purposes, the area of I(12,3) is assumed equal to that of erythrocyte lipid. Probe molecules are represented by [■], while white space is erythrocyte lipid. Ratios of 'dilute' to 'concentrated' spins in the resonant portion of the cavity for lipid/probe of 4600, 359, 90 and 26 are: $1.2 \times 10^{14}/0$, $6.7 \times 10^{14}/5.3 \times 10^{14}$, $3.0 \times 10^{14}/3.56 \times 10^{15}$ and $1.09 \times 10^{13}/1.63 \times 10^{16}$, respectively

Spin-Probe Clustering in Human Erythrocyte Ghosts According to Model II

If the number of spins present in concentrated spectra is equal to clustered I(12,3), then subtraction of 'low-range' spectra from 'intermediate-range' spectra readily yields the dilute/clustered probe ratio. I(12,3) segregation in erythrocyte ghosts may now be assessed using Model II as a function of either P/L or μg I(12,3)/mg protein. Figure 14 shows that significant clustering occurs at P/L of 1/359 to 1/2250, and that at 1/100, over 85% of the probe is segregated. These results are illustrated in Fig. 15*A-D*, where the relative proportions of both dilute and clustered probe in erythrocyte lipid are shown schematically. Both the absolute and relative amounts of 'magnetically dilute' I(12,3) sites decrease with increasing P/L.

Probe Distribution Model III: Rapid Lateral Diffusion of Homogeneously Distributed I(12,3) in Erythrocyte Membranes

I(12,3) is assumed to partition uniformly in bulk-membrane lipid at 37°C, and the spectral broadening would therefore be principally due to spin-exchange between probe molecules which collide when executing rapid lateral diffusion. Following Model III, a lateral diffusion coefficient (L_D) of 3×10^{-7} cm^2/sec for I(12,3) in erythrocyte membranes may be calculated from the ΔH broadening of Fig. 4*A* [37].

Model III is unlikely to provide an accurate description of I(12,3) distribution and dynamics in erythrocyte ghosts. The above L_D would rank erythrocytes as one of the most fluid biological membranes ever examined [26]. This picture disagrees with our earlier finding that I(12,3)-labeled erythrocytes are one of the least fluid membranes, as assessed by order parameters sensitive to probe flexibility [16, 17, 35]. Also inconsistent with Model III are the low L_D detected for either integral membrane proteins ($<3 \times 10^{-12}$ cm^2/sec) [26] or incorporated fluorescent probes diI, NBD-PE or NBD-Chol ($\sim 2 \times 10^{-9}$ cm^2/sec) [15, 38]. Lastly, Model III, which views the interaction of I(12,3) with ghosts as a partitioning phenomenon, does not readily explain probe binding to high-affinity sites at low loading (Fig. 2*B*).

Conclusions

In human erythrocyte ghosts, the best description of I(12,3) distribution and spectral changes with increasing probe concentration is provided by Model II. I(12,3) binds to high-affinity sites to yield 'magnetically dilute' spectra at low P/L. Saturation occurs with increasing P/L and, at high loading, occupied sites act as nuclei for insertion of additional probe. The affinity of occupied sites for I(12,3) is much less than that of unoccupied sites at low P/L. Low association constants at high P/L may be due either to steric hinderance offered by occupied sites or to high local concentrations of negatively charged probe which repel additional I(12,3). In the intermediate-range, spectra are composites reflecting 'dilute' probe exchanging slowly on an ESR time-scale with membrane-bound clustered (or 'concentrated') probe. The above model accounts well for the data presented here. It explains why spectral broadening due to probe-probe interactions (Figs. 3*b-g*, 4) occurs over the same P/L range as that over which I(12,3) binding precipitously declines (Fig. 2). Application of Model II not only allows deconvolution of intermediate-range spectra into 'dilute' and 'concentrated' components, but also permits accurate simulation of spectral features observed experimentally at high loading (Figs. 6-11). Consistent with the model's prediction that 'dilute' sites will be lost at high P/L, the ratio of 'dilute' to 'concentrated' decreases dramatically (Fig. 14) over the same range where high-affinity sites are saturated (Fig. 2) and probe-probe interactions are manifest (Fig. 4).

An important finding centers on our observation that significant I(12,3) clustering occurs at much lower P/L (e.g., 1/2250 to 1/359) than has been previously reported [5, 16]. This is a radical departure from the conventional picture of 'magnetically dilute' I(12,3) located in a homogeneous fluid phase for P/L $<1/100$. One explanation for the discrepancy is the incorrect assumption of Butterfield et al. [5] and Gordon and Mobley [16] that erythrocyte membranes quantitatively incorporated I(12,3) over the entire P/L range. Figure 2 indicates that such an assumption leads to a serious overestimation of the probe concentration in the membrane. A second reason is our inability to readily discern heterogeneity in the ESR spectra due to probe segregation (e.g., Fig. 3*b-g*). This is attributed to overlap between the spectral components of both the dilute and clustered probe, becoming particularly severe at the low end of the intermediate range. Only when 'low' and 'concentrated' spectra have been isolated does the broadening become obvious (e.g., Figs. 6*a,b,i*; 7*a,b,i*).

Although the above data were obtained with erythrocyte ghosts, there seems to be no reason why Model II could not be applied to other membranes exhibiting similar spectral alterations with increasing I(12,3) concentration (*see* Introduction). In the sinusoidal sub-fraction purified from rat liver plasma membranes, we have observed marked re-

duction in I(12,3) uptake over the same P/L range as that in which probe-probe interactions occur (N. Osman, R. LePaige, F. Looney, C. C. Curtain, L. Gordon, *unpublished observations*).

The phenomenon of I(12,3) clustering in human erythrocyte ghosts at 37°C broadly agrees with earlier spin-label studies. A phase of enriched phospholipid spin probe separated out below 20°C in sarcoplasmic reticulum [36] while clustering of either the androstane or I(12,3) spin probe was detected in dipalmitoyllecithin below the transition temperature [23, 32]. Such probe sequestration may be a characteristic marker of thermotropic phase separations (or transitions) involving endogenous lipids. Certainly, the present findings support our assignment with erythrocyte membranes that enhanced radical interactions below the high onset of the lipid phase separation are due to greater I(12,3) clustering [16].

It is of interest to consider high-affinity binding sites for I(12,3) in erythrocyte membranes. From probe titrations, a 'magnetically dilute' S of 0.640 is calculated from low-range spectra (Fig. 4*A*). These results indicate that I(12,3), when occupying high-affinity sites, exhibits rapid anisotropic motion about its long axis and limited chain flexibility. Since 100% of high-affinity sites are saturated with I(12,3) at P/L = 1/359, ESR spectra of occupied sites will not necessarily reflect properties of bulk lipid. The limited number of high-affinity sites (Fig. 2*B*) suggests that labeled micro-domains reflect defective regions in the bilayer (e.g., liquid-lipid domains or grain boundaries between domains) where I(12,3) incorporates with little steric hinderance and high avidity. This would agree with the preferential distribution of fatty-acid spin probes into the more fluid phase of mixed model bilayers [3]. High-affinity sites probably reflect cholesterol-poor domains, since cholesterol enrichment of I(12,3)-labeled rat liver plasma membranes promoted probe clustering as indicated by empirical parameters sensitive to probe interactions [16, 18]. One possibility worth exploring is that 'dilute' spectra are due, at least partially, to I(12,3) binding to integral membrane proteins as 'annular' lipid. This may be tested by repeating the present experiments with either lipid-extracts of erythrocytes or model lipids mimicking the composition of erythrocytes.

If I(12,3) does not distribute uniformly in erythrocyte ghosts and other membranes, there is some question as to whether the 'dilute' spectral parameters will yield relevant information on structure and function. Instances are readily envisioned in which sequestered probe is unable to sense lipid domains that regulate membrane activities; conversely, spectral changes detected by the localized probe would not necessarily reflect distal membrane functions. Nevertheless, there is now considerable evidence indicating that the activities of numerous membrane enzymes are influenced by lipid domains sampled by I(12,3) [17, 21, 25]. This conclusion was arrived at by manipulating the lipid composition/fluidity with various agents, and then concurrently determining enzyme activities and order parameters. Although 'dilute' S will probably provide information on functionally significant lipid regions, the inhomogeneous I(12,3) distribution reported here suggests that a complete profile of constituent domains will emerge only if spin probes that closely approximate endogenous components (e.g., phospholipid and glycolipid spin probes) are also used [7].

A frequent criticism of membrane ESR spectroscopy studies is that the spin probe is a foreign molecule and its introduction perturbs the bilayer to an unknown extent. Certainly, incubation of intact erythrocytes with I(12,3) induces echinocyte morphology and cell lysis at probe concentrations of 10^{-8} and 10^{-5} M [2]. In this context, the 'concentrated' component isolated in the intermediate range undoubtedly represents probe in a distorted environment. The broadened spectra of Fig. 12 demonstrate that 'concentrated' domains are increasingly enriched in the fatty-acid spin probe with higher P/L. Furthermore, raising the level of bound I(12,3) becomes increasingly difficult above a P/L of 1/359, suggesting that perturbation of the binding sites must be accomplished before additional probe will insert into the bilayer. On the other hand, I(12,3) binding in the low-range is believed to minimally distort the membrane for several reasons. First, high-affinity site occupation at low loading involves I(12,3) molecules that are not in van der Waal's contact. Second, the avidity for I(12,3) at low P/L suggests that high-affinity binding is due to already expanded sites (e.g., liquid-lipid domains) that readily accommodate I(12,3) with its bulky oxazolidine ring. It should also be pointed out that any perturbations present in the 'concentrated' component are not transmitted to the 'dilute' component of the intermediate-range spectra. Otherwise, accurate simulation of spectral alterations could not be achieved with Model II. Deconvolution into 'dilute' and 'concentrated' components provides us with an internal monitor that rules out gross membrane perturbations in the intermediate range. However, we have no such assurance when 'dilute' is lost at higher P/L (e.g., Fig. 3*h,i*), and I(12,3) may well exert widespread, detergent-like effects.

The present studies emphasize that "intrinsic" membrane properties (e.g., S) cannot be evaluated unless spectra independent of probe-probe interac-

tions are measured.[2] This requires that titrations be carried out for each system to the limits of instrument sensitivity. Without such titrations, errors may be introduced into the determination of $2T_\perp$, S and a'_N (Fig. 4). It is of particular interest that significant I(12,3) clustering occurs in erythrocyte membranes at what otherwise might be thought to be low probe/*total lipid* ratios (i.e., $1/2250 \leq P/L \leq 1/359$). Clearly, attempts to rigorously analyze the spectra of $I(m,n)$-labeled membranes in terms of motional models [22] may lead to artifactual results, unless 'magnetically dilute' spectra are first established from probe titrations and the spectral subtraction method of Model II. However, the empirical analysis used in Model II is limited to the extent that the spin probe concentration in the 'concentrated' component is ill-defined. It will be of much interest in future studies to learn if the experimental spectra can be theoretically simulated by first generating exchange-broadened spectra using various encounter frequencies and then adding nonexchange broadened components [27].

Complementary views of probe-probe interactions are provided by empirical parameters and percentages of 'clustered' probe obtained from Model II. Changes in empirical parameters at high P/L are due to two factors: loss of 'dilute' spectra (e.g., Figs. 9, 10*D*) and increased radical interactions in the 'concentrated' component (Figs. 12, 13). The ratio of 'dilute' to 'clustered' probe is most accurate in quantitating probe sequestration at very low P/L, while empirical parameters are more useful at higher loading where % clustering approaches 100. The sensitivity of empirical parameters to probe-probe interactions is as follows: $h_{-1}/h_0 > \Delta H > S(T_\perp) > m$. Simultaneous use of empirical parameters and Model II provides us with tools to evaluate radical interactions over the entire P/L range.

Since probe clustering may be indicative of rearrangements of native lipid, the spectral subtraction method outlined here should be useful in quantitating such redistributions. Previously, we have used empirical parameters developed by Sauerheber et al. [33] and Gordon et al. [20] to estimate lipid domain formation and condensation phenomena in biological membranes. For example, mitogenic stimulation of lymphocytes induces clustering of labeled glycospingolipids [8, 10]; such lipid redistributions may be a key event in triggering lymphoid cell activation [6]. These empirical parameters have also been used to assign thermotropic lipid phase separations in rat liver and heart plasma membranes [18, 20], human platelet plasma membranes [18], and human erythrocyte ghosts [16], and have indicated cholesterol-rich and -poor domains in rat liver plasma membranes [16, 18]. Now, it should be possible with Model II to accurately determine proportions of clustered probe in the above systems and to show whether 'clustered' probe perturbs the environment of 'dilute' probe.

[2] Here, "intrinsic" properties are defined as those which are measured when probe interactions are negligible, and do not refer to membrane behavior in the absence of a perturbing label [33].

Dr. L.M. Gordon was a Visiting Scientist of the Division of Chemical and Wood Technology, CSIRO (Jan.–Mar., 1984). This work was sponsored by grants-in-aid from the American Diabetes Association, Southern California Affiliate, Inc., the Juvenile Diabetes Foundation, National Institutes of Health grant HL/AM-27120, and the California Metabolic Research Foundation. We thank the reviewers for useful comments.

References

1. Amatruda, J.M., Finch, F.D. 1979. Modulation of hexose uptake and insulin action by cell membrane fluidity. *J. Biol. Chem.* **254**:2619–2625
2. Bieri, V., Wallach, D.F.H., Lin, P. 1974. Focal erythrocyte membrane perturbations caused by nitroxide lipid analogues. *Proc. Natl. Acad. Sci. USA* **71**:4797–4801
3. Butler, K.W., Tattrie, N.H., Smith, I.C.P. 1974. The location of spin probes in two phase mixed lipid systems. *Biochim. Biophys. Acta* **363**:351–360
4. Butler, K.W., Deslauriers, R., Smith, I.C.P. 1984. *Plasmodium berghei:* Electron spin resonance and lipid analysis of infected mouse erythrocyte membranes. *Exp. Parasitol.* **57**:178–184
5. Butterfield, D.A., Whisnant, C.C., Chesnut, D.B. 1976. On the use of the spin labeling technique in the study of erythrocyte membranes. *Biochim. Biophys. Acta* **426**:697–702
6. Curtain, C.C. 1984. Glycosphingolipid domain formation and lymphocyte activation. *In:* Biomembranes. M. Kates and L. Manson, editors. Vol. 12, pp. 603–632. Plenum, New York
7. Curtain, C.C., Gordon, L.M. 1984. Membrane ESR spectroscopy. *In:* Membranes, Detergents, and Receptor Solubilization. J.C. Venter and L. Harrison, editors. Vol. 1, pp. 177–213. Alan R. Liss, New York
8. Curtain, C.C., Looney, F.D., Marchalonis, J.J., Raison, J.K. 1978. Changes in lipid ordering and state of aggregation in lymphocyte plasma membranes after exposure to mitogens. *J. Membrane Biol.* **44**:211–232
9. Curtain, C.C., Looney, F.D., Regan, D.L., Ivancic, N.M. 1983. Changes in the ordering of lipids in the membrane of *Dunaliella* in response to osmotic-pressure changes. *Biochem. J.* **213**:131–136
10. Curtain, C.C., Looney, F.D., Smelstorius, J.A. 1980. Lipid domain formation and ligand-induced lymphocyte membrane changes. *Biochim. Biophys. Acta* **596**:43–56
11. Curtain, C.C., Looney, F.D., Smelstorius, J.A. 1981. Glycosphingolipid clustering and mast cell degranulation. *Int. Arch. Appl. Immunol.* **65**:34–41
12. Dodge, J.T., Mitchell, C., Hanahan, D.J. 1963. The preparation and characterization of hemoglobin-free ghosts of human erythrocytes. *Arch. Biochem. Biophys.* **100**:119–130

13. Elgavish, A., Rifkind, J., Sacktor, B. 1983. In vitro effects of vitamin D_3 on the phospholipids of isolated renal brush border membranes. *J. Membrane Biol.* **72:**85–91
14. Gaffney, B.J. 1974. Spin-label measurements in membranes. *Methods Enzymol.* **32B:**161–198
15. Golan, D.E., Alecio, M.R., Veatch, W.R., Rando, R.R. 1984. Lateral mobility of phospholipid and cholesterol in human erythrocyte membrane: Effects of protein-lipid interactions. *Biochemistry* **23:**332–339
16. Gordon, L.M., Mobley, P.W. 1984. Thermotropic lipid phase separations in human erythrocyte ghosts and cholesterol-enriched rat liver plasma membranes. *J. Membrane Biol.* **79:**75–86
17. Gordon, L.M., Mobley, P.W. 1985. Membrane lipids, membrane fluidity and enzyme activity. *In:* Membrane Fluidity in Biology. R.C. Aloia and J. Boggs, editors. Vol. IV. Academic, New York (*in press*)
18. Gordon, L.M., Mobley, P.W., Esgate, J.A., Hofmann, G., Whetton, A.D., Houslay, M.D. 1983. Thermotropic lipid phase separations in human platelet and rat liver plasma membranes. *J. Membrane Biol.* **76:**139–149
19. Gordon, L.M., Sauerheber, R.D. 1977. Studies on spin-labelled egg lecithin dispersions. *Biochim. Biophys. Acta* **466:**34–43
20. Gordon, L.M., Sauerheber, R.D., Esgate, J.A. 1978. Spin-label studies on rat liver and heart plasma membranes: Effects of temperature, calcium and lanthanum on membrane fluidity. *J. Supramol. Struct.* **9:**299–326
21. Gordon, L.M., Sauerheber, R.D., Esgate, J.A., Dipple, I., Marchmont, R.J., Houslay, M.D. 1980. The increase in bilayer fluidity of rat liver plasma membranes achieved by the local anesthetic benzyl alcohol affects the activity of intrinsic membrane enzymes. *J. Biol. Chem.* **255:**4519–4527
22. Griffith, O.H., Jost, P.C. 1976. Lipid spin labels in biological membranes. *In:* Spin Labeling. Theory and Applications. L. Berliner, editor. Chap. 7, pp. 453–523. Academic, London
23. Hauser, H., Guyer, W., Howell, K. 1979. Lateral distribution of negatively charged lipids in lecithin membranes. Clustering of fatty acids. *Biochemistry* **18:**3285–3291
24. Horvath, L.I., Bagyinka, C.S., Sandor, M., Gergely, J. 1982. Changes in the lateral ordering of the macrophage plasma membrane during Fc receptor mediated phagocytosis. *Mol. Immunol.* **19:**1603–1610
25. Houslay, M.D., Gordon, L.M. 1983. The activity of adenylate cyclase is regulated by the nature of its lipid environment. *Curr. Top. Membr. Transp.* **18:**179–231
26. Houslay, M.D., Stanley, K.K. 1982. Dynamics of Biological Membranes. pp. 1–33. Wiley, New York
27. Humphries, G.M.K., McConnell, H.M. 1982. Nitroxide spin labels. *In:* Methods of Experimental Physics. R. Favia, editor. Vol. 20, pp. 53–122. Academic, New York
28. Koszo, F., Horvath, L.I., Simon, N., Siklosi, C.S., Kiss, M. 1982. The role of possible membrane damage in porphyrin cutanea tarda: A spin-label study of rat liver cell membranes. *Biochem. Pharmacol.* **31:**11–17
29. Merritt, M.V., Loughman, B.E. 1979. Spin labeling studies of the interaction of P815 mouse mastocytoma cells with antisera to histocompatibility antigen, H-2d. *Immunopharmacology* **1:**301–314
30. Pauls, K.P., Thompson, J.E., Lepock, J.R. 1980. Spin label studies of microsomal membranes from *Acanthamoeba castellanii* in different states of differentiation. *Arch. Biochem. Biophys.* **200:**22–30
31. Puskin, J.S., Wiese, M.B. 1982. A spin label study of human lens membranes. *Exp. Eye Res.* **35:**251–258
32. Sackmann, E., Trauble, H. 1972. Studies of the crystalline-liquid crystalline phase transition of lipid model membranes. *J. Am. Chem. Soc.* **94:**4482–4491
33. Sauerheber, R.D., Gordon, L.M., Crosland, R.D., Kuwahara, M.D. 1977. Spin-label studies on rat liver and heart plasma membranes: Do probe-probe interactions interfere with the measurement of membrane properties? *J. Membrane Biol.* **31:**131–169
34. Sauerheber, R.D., Lewis, U.J., Esgate, J.A., Gordon, L.M. 1980. Effects of calcium, insulin and growth hormone on membrane fluidity. A spin label study of rat adipocyte and human erythrocyte ghosts. *Biochim. Biophys. Acta* **597:**292–304
35. Sauerheber, R.D., Zimmerman, T.S., Esgate, J.A., Vanderlaan, W.P., Gordon, L.M. 1980. Effects of calcium, lanthanum and temperature on the fluidity of spin-labeled human platelets. *J. Membrane Biol.* **52:**201–219
36. Scandella, C.J., Devaux, P., McConnell, H.M. 1972. Rapid lateral diffusion of phospholipids in rabbit sarcoplasmic reticulum. *Proc. Natl. Acad. Sci. USA* **69:**2056–2060
37. Stier, A., Sackmann, E. 1973. Spin labels as enzyme substrates. Heterogeneous lipid distribution in liver microsomal membranes. *Biochim. Biophys. Acta* **311:**400–408
38. Thompson, N.L., Axelrod, D. 1980. Reduced lateral mobility of a fluorescent lipid probe in cholesterol-depleted erythrocyte membranes. *Biochim. Biophys. Acta* **597:**155–165
39. Verma, S.P., Wallach, D.F.H. 1975. Evidence for constrained lipid mobility in the erythrocyte ghost. A spin-label study. *Biochim. Biophys. Acta* **382:**73–82

Received 13 July 1984; revised 12 October 1984